Title: **Baseline-Subtraction-Free (BSF) Damage-Scattered Wave Extraction for Stiffened Isotropic Plates**

Authors : Jiaze He[1]
Patrick E. Leser[2]
William P. Leser[3]

ABSTRACT

Lamb waves enable long distance inspection of structures for health monitoring purposes. However, this capability is diminished when applied to complex structures where damage-scattered waves are often buried by scattering from various structural components or boundaries in the time-space domain. Here, a baseline-subtraction-free (BSF) inspection concept based on the Radon transform (RT) is proposed to identify and separate these scattered waves from those scattered by damage. The received time-space domain signals can be converted into the Radon domain, in which the scattered signals from structural components are suppressed into relatively small regions such that damage-scattered signals can be identified and extracted. In this study, a piezoelectric wafer and a linear scan via laser Doppler vibrometer (LDV) were used to excite and acquire the Lamb-wave signals in an aluminum plate with multiple stiffeners. Linear and inverse linear Radon transform algorithms were applied to the direct measurements. The results demonstrate the effectiveness of the Radon transform as a reliable extraction tool for damage-scattered waves in a stiffened aluminum plate and also suggest the possibility of generalizing this technique for application to a wide variety of complex, large-area structures.

INTRODUCTION

Guided waves have been studied for damage detection in large-area structures for both nondestructive evaluation (NDE) and structural health monitoring (SHM) purposes [1,2]. While the long distance propagation property of Lamb waves is preferable for fast inspection, it can result in additional complexities due to scattering induced by structural boundaries and structural components, such as stiffeners and holes [3]. Thus, damage-scattered waves are often buried in the time-space domain.

One of the most common solutions to this problem is to use a baseline-subtraction such that the difference between the newly measured signals and baseline signals are

[1]Jiaze He, National Institute of Aerospace, Hampton, VA 23666 U.S.A.. Email: jiaze.he@nianet.org; North Carolina State University, Raleigh, NC, 27695 U.S.A.. Email: jhe7@ncsu.edu
[2]Patrick E. Leser, NASA Langley Research Center, Hampton, VA 23618 U.S.A..
[3]William P. Leser, NASA Langley Research Center, Hampton, VA 23618 U.S.A..

assumed to be the damage-induced signals [4]. However, the environmental factors (e.g. temperature variation) and operational variability could invalidate the baseline [5]. An instantaneous baseline [6] can be obtained through a comparison between different sensor pairs that have similar path, but if the sensor pairs have different positions relative to various structural components, obtaining the instantaneous baseline is difficult. If ultrasonic guided waves are used for inspection in a one-dimensional (1-D) mode [7], it is possible to extract more information without a baseline in the time-frequency domain. However, the two-dimensional (2-D) areal inspection capability of guided waves is abandoned such that the scanning process will be relatively slow, limiting the applicability to SHM.

Wang and Yuan [8] proposed a baseline-free lead zirconate titanate (PZT) sensor arrangement in which an actuator and sensor pair are placed close to each other in order to increase the time difference between direct arrival signals and scattered signals. Reflections from structural components and the direct arrival signals were removed, for the situation where the degree of overlap is small. However, separating the scattered signals can still prove difficult if a damage site is located close to the sensing pair or boundaries of the plate.

Based on the spatial reciprocity and time reversal invariance of the linear wave equations, a time-reversal process was developed for reconstructing Lamb wave signals from a sensing pair on plates [9]. If the reconstruction cannot be done, it is assumed that damage exists at the possible paths between sensing pairs. This method is baseline-free; however, it provides only one value for the entire route between a sensing pair such that most of the temporal information and the 2-D capability of guided waves are not fully utilized.

In this paper, a Radon transform (RT) is proposed to recognize and extract severely buried, damage-scattered signals in large-scale complex structures without baseline-subtraction. In geophysics, Radon transforms have been widely used for dispersion curve plotting [10], multi-mode wavefield separation [11], and demultiples (removal of multiple reflections) [12]. A linear radon transform has been applied to plot and estimate the dispersion relations for guided waves in aluminum plates [13] and long bones [14]. However, limited studies were found on damage-scattered signal separation using Lamb waves for NDE and SHM.

THEORY

The data acquisition configuration used in this research is shown in Fig. 1. Here an actuator sends out a signal and a group of receivers are used to record the signals. This setup is similar to the linear arrays that are commonly used in SHM or NDE [15–17].

The (conventional) discrete forward linear Radon transform from the time-space (t - x) domain to the intercept-slowness (τ - p) domain is achieved through summation along the straight line $t = \tau + px$ [5, 11],

$$m(\tau, p_k) = \sum_{j=0}^{N-1} d(t = \tau + p_k x_j, x_j),\ k = 0, ..., K-1, \tag{1}$$

where $d(t, x_j)$ denotes the time-space domain signals, x_j is the receiver location, $m(\tau, p_k)$

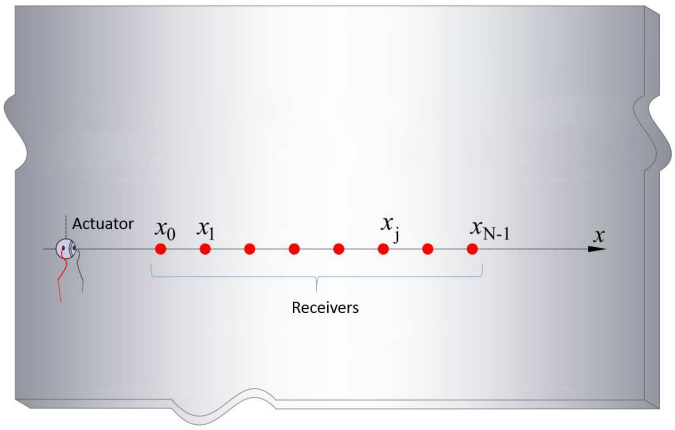

Figure 1. Signal acquisition setup

represents the τ - p domain signals, τ is the intercept time, p is the ray parameter, N is the number of sensors and K is the number of sampled ray parameters. Thus, the conversion is also referred to as the τ - p or slant-stack transform. Similarly, the inverse Radon transform can be written as:

$$d(t, x_j) = \sum_{k=0}^{K-1} m(\tau = t - p_k x_j, p_k),\ j = 0, ..., N-1. \tag{2}$$

The frequency representation is easier to implement than using time-domain representation. Taking the temporal Fourier transform (FT) of Eq. 2 yields

$$D(\omega, x_j) = \sum_{k=0}^{K-1} M(\omega, p_k) e^{-i\omega p_k x_j}. \tag{3}$$

Eq. 3 can be simplified using matrix notation for each frequency

$$\mathbf{D} = \mathbf{L}\mathbf{M}, \tag{4}$$

with $L_{jk} = e^{-i\omega p_k x_j}$, $k = 0, ..., K-1$, and $j = 0, ..., N-1$ Then the frequency representation of Eq. 1 can be expressed as

$$\mathbf{M} = \mathbf{L}^{\mathbf{H}}\mathbf{D}. \tag{5}$$

$\mathbf{H}$ denotes the conjugate transpose operation. However, $\mathbf{L}$ and $\mathbf{L}^{\mathbf{H}}$ do not form a perfect inverse pair, which means

$$\mathbf{D} \neq \mathbf{L}\mathbf{L}^{\mathbf{H}}\mathbf{D}. \tag{6}$$

To find a least-square (LS) solution of M in Eq. 4, a common method [18] is to minimize the following cost function

$$J = \|\mathbf{D} - \mathbf{L}\mathbf{M}\| + \mu\|\mathbf{M}\|^2, \tag{7}$$

where μ is a damping parameter. Then $\mathbf{M}$ can be estimated by taking the derivatives of J to form the damped least-square (DLS) solution

$$\mathbf{M} = (\mathbf{L}^{\mathbf{H}}\mathbf{L} + \mu\mathbf{I})^{-1}\mathbf{L}^{\mathbf{H}}\mathbf{D}. \tag{8}$$

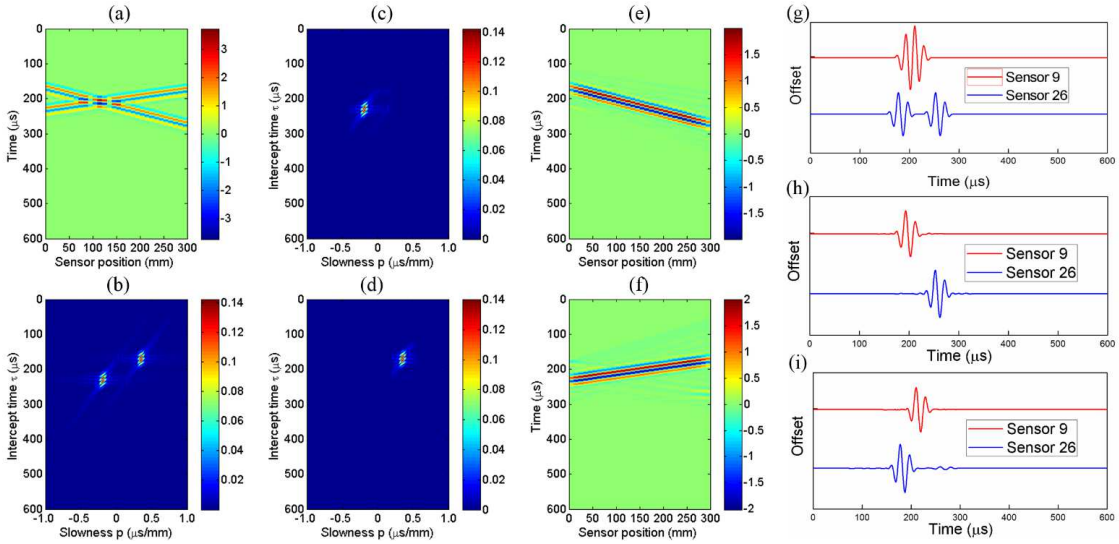

Figure 2. Two simulated, linear events in (a) the t - x domain and (b) the τ - p domain, along with the separated signals in the τ - p domain from (c) S1 and (d) S2. The signals from (c-d) were also converted back to the t - x domain for (e) S1 and (f) S2. (g-i) The signals as received by sensors 9 and 26 corresponding to the three cases in (a), (e) and (f) are shown in (g), (h), and (i), respectively.

Eq. 8 and Eq. 4 are the forward and inverse Radon operator pair in the frequency domain. The t - x domain signals can be obtained by taking the inverse temporal FT of Eq. 8.

WAVE SEPARATION ILLUSTRATION

In order to demonstrate the wave separation process and test the algorithm's effectiveness, a 1D example was investigated (Fig. 2). Three-cycled Hanning-windowed toneburst signals were excited at two separate sources, S1 and S2, which were located at x = 0 and x = 290 mm, respectively. This signal type is one of the most commonly used for ultrasonic guided wave-based SHM. A linear sensor array was distributed between S1 and S2. Thirty sensors were used with locations ranging from $x = 0$ to $x = 290$ mm and uniform spacing of 10 mm. The signals emitted from S1 and S2 started at 140 and 200 μs and traveled with slowness -0.35 and 0.2 $\mu\mathrm{s/mm}$, respectively. The response at all 30 sensors resulting from the events at S1 and S2 is shown in Fig. 2(a). The linear Radon transform of these simulated signals is shown in Fig. 2(b), where the two linear events in the time-space domain have been compressed into two point-like areas in the τ - p domain.

The response signals from several sensors overlap, as indicated in Fig. 2(a) by the overlapping bands between the approximate positions of 90 and 150 mm. To separate the two events in the Radon domain, windows of $[170 - 300\ \mu\mathrm{s}] \times [-0.4 - 0.2\ \mu\mathrm{s/mm}]$ and $[120 - 230\ \mu\mathrm{s}] \times [0.2 - 0.55\ \mu\mathrm{s/mm}]$ were applied in the τ - p domain. Separating these windows resulted in Fig. 2(c) and Fig. 2(d), respectively. Taking the inverse Radon transform, the received response from each event can be converted back to the

t - x domain as shown in Fig. 2(e) and Fig. 2(f). The two events were well separated and the overlapping components in Fig. 2(a) were recovered. For further illustration, the unmodified response signals (Fig. 2(a)) received at Sensor 9 and 26 are shown in Fig. 2(g); the overlap is clearly seen for Sensor 9. Using the separated responses from Fig. 2(e) and Fig. 2(f), the separated signals at Sensor 9 and 26 were plotted in Fig. 2(h) and Fig. 2(i), respectively. The overlapped region was resolved and the signals resulting from each of the individual events are obtained.

EXPERIMENTAL VERIFICATION

The results of this simple study encouraged exploration of similar applications, particularly those pertaining to damage-scattered wave separation for SHM and NDE purposes. To this end, the setup described in Fig. 1 was utilized for Lamb wave generation and reception in a stiffened, aluminum alloy 6013-T6 plate as shown in Fig. 3(a). The system consisted of a function generator (Tek AFG3000), a power amplifier (Krohn-Hite 7602), a LDV (Polytec OFV-505), and a 2D translational stage (IAI ROBO). The laser pointed at the plate perpendicularly in order to measure the out-of-plane velocity. The aluminum plate had dimensions of 753 mm $\times$ 612 mm $\times$ 4.9 mm.

The actuator used in this research was a piezoelectric wafer (Steiner & Martins, Inc.) with dimensions of 7 mm in diameter and 0.3 mm in thickness. The origin (0, 0) of the coordinate system was located at the center of the piezoelectric wafer, which was 21.5 mm to the left of a rib (Fig. 3(c)). Artificial damage was introduced using a pair of rectangular magnets of length 19.1 mm and width 12.7 mm. The magnets were mounted on either side of the plate at (40.5, 91.4) mm.

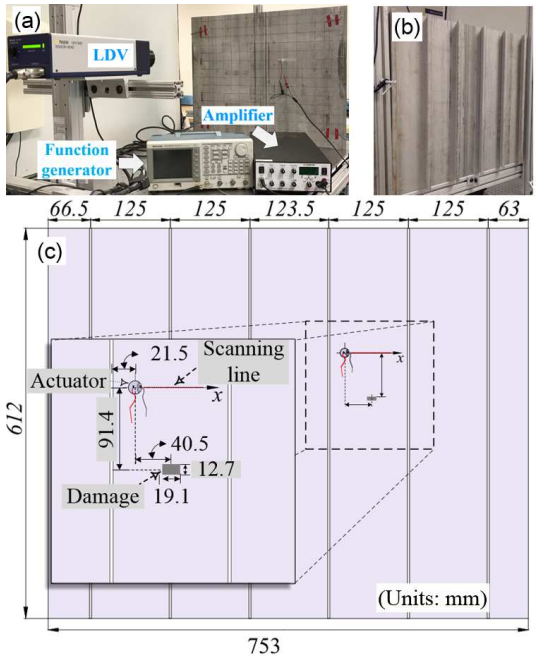

Figure 3. Experimental setup (a) front view, (b) back view, and (c) diagram of the area of interest.

A linear scan was conducted from x=10 mm to 80 mm with a spacing of 2 mm. At each scanning point, 10 measurements were taken to increase the signal to noise ratio (SNR). The input signal was a 2.5-cycle Hanning-windowed tone-burst signal with a center frequency of 30 kHz. With this frequency, the excited A_0 mode waves had a much larger amplitude compared with the S_0 mode waves.

The received signals without artificial damage are shown in Fig. 4(a). These signals represent the baseline, which is typically a necessity for guided wave-based SHM, especially for a structure of this complexity. The magnet pair was attached to the panel at the denoted location, and the corresponding received signals for the now damaged panel are shown in Fig. 4(b); these signals will be referred to as those obtained from the damaged state.

Since the scattering from the stiffeners was extremely complicated, the damage-scattered signals could not be identified from the current signals, let alone separated from the baseline signals. This is the major reason that most current guided wave-based damage imaging technologies for SHM require a baseline. Applying the common baseline-subtraction procedure yielded the damage-scattered signals shown in Fig. 4(c), which can be used for damage imaging. However, due to temperature changes and other possible environmental variations, the baseline process is often either not applicable or intractable due to the requirement of a baseline for all potential variations [5].

The main purpose of this paper is to illustrate that, operating directly on signals in Fig. 4(b), the damage-scattered signals can be recognized and separated using the Radon transform. Applying the DLS RT to the signals in Fig. 4(a), the τ - p domain was obtained as shown in Fig. 4(d). Compared with the signals in the t - x domain, the signals in the τ - p domain are more condensed. Thus, once damage is introduced, if the damage-scattered signals in the τ - p domain correspond to any of the remaining area (i.e., regions of the τ - p domain that do not already possess large amplitude wave components), it is possible to recognize and isolate the damage-scattered signals.

The DLS RT was applied to signals from the damaged state shown in Fig. 4(b), resulting in the τ - p domain shown in Fig. 4(e). By comparing the "empty" regions in the τ - p domain of the baseline (Fig. 4(d)) with the τ - p domain of the damaged state (Fig. 4(e)), new features can be identified that are assumed to correspond to the addition of damage. A rectangular window was used to isolate this region (the bottom right box shown in Fig. 4(e)). This isolated region was converted back to the t - x domain as shown in Fig. 4(f). Comparing these signals, which were obtained without baseline subtraction, to those obtained using baseline subtraction in Fig. 4(c), the major parts of the damage-scattered signals were all recovered.

A slight difference in shape can be observed in the recovered, damage-scattered signal when compared to the baseline subtraction result. This is likely due to the choice of the window used to separate the events in the τ - p domain. The rectangular window likely cut off a small part of the signal in this domain, resulting in a loss of information. These excluded parts correspond to the well-studied "near-offset" and "far-offset" artifacts. [19] One way to address the aforementioned issue is to use the high resolution Radon transform (HRRT) to suppress the artifacts [11]. The HRRT signals in the τ - p domain leave more space that can be used for damage-scattered signal separation, allowing for improved rectangular windowing. Additionally, automatic methods for arbitrary window selection based on the available space in the τ - p domain could also alleviate

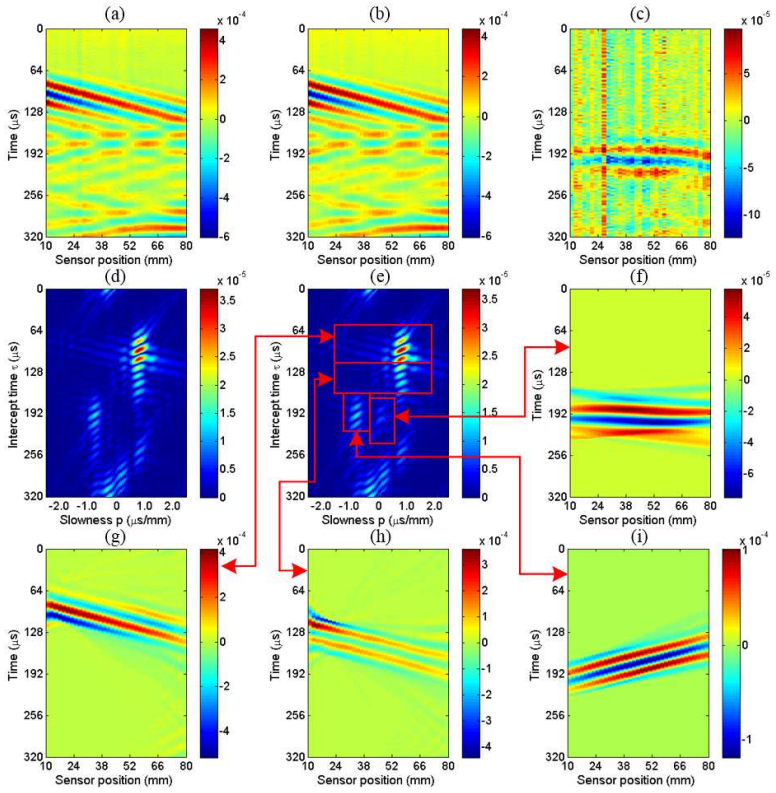

Figure 4. Signals in the t - x domain from (a) the baseline and (b) the damaged state, (c) damage-scattered signals in the t - x domain obtained using baseline subtraction, (d) baseline and (e) damaged state signals in the τ - p domain, (f) damage-scattered signals in the t - x domain obtained using the Radon transform (i.e., without baseline subtraction), and (g-i) the t - x domain signals extracted from the damaged state corresponding to the direct-arrivals from the actuator, the reflection from the left rib, and the reflection from the right rib, respectively.

this issue. This research is currently ongoing.

A similar process was employed to isolate the remaining event responses in the damaged state τ - p domain. Three more rectangular windows were used, as shown in Fig. 4(e). Due to the known relative positions between the array and ribs, the corresponding results in the t - x domain can be easily recognized as the recovery of (g) the direct-arrival from the actuator, (h) the reflection from the left rib, and (i) the reflection from the right rib. The exercise shows that the proposed technique can also be used to separate and study the primaries from the actuator and the scattering from other structural components.

CONCLUDING REMARKS

In conclusion, the proposed Radon transform technique can be used for baseline-subtraction-free (BSF) damage-scattered wave recognition and extraction for ultrasonic guided wave-based SHM or NDE purposes in large-scale complex structures.

The authors acknowledge the support provided by National Institute of Aerospace's IRAD funding: Scattered Wave Extraction (I207).

REFERENCES

1. Dalton, R., P. Cawley, and M. Lowe. 2001. "The potential of guided waves for monitoring large areas of metallic aircraft fuselage structure," *J. Nondestruct. Eval.*, 20(1):29–46.
2. Pruell, C., J.-Y. Kim, J. Qu, and L. J. Jacobs. 2007. "Evaluation of plasticity driven material damage using Lamb waves," *Appl. Phys. Lett.*, 91(23):231911.
3. Kim, S. B., C. G. Lee, J.-W. Hong, H. W. Park, and H. Sohn. 2010. "Applications of an instantaneous damage detection technique to plates with additional complexities," *J. Nondestruct. Eval.*, 29(3):189–205.
4. Ihn, J.-B. and F.-K. Chang. 2008. "Pitch-catch active sensing methods in structural health monitoring for aircraft structures," *Struct. Health. Monit.*, 7(1):5–19.
5. Wang, D., L. Ye, Y. Lu, and F. Li. 2010. "A damage diagnostic imaging algorithm based on the quantitative comparison of Lamb wave signals," *Smart. Mater. Struct.*, 19(6):065008.
6. Anton, S. R., D. J. Inman, and G. Park. 2009. "Reference-free damage detection using instantaneous baseline measurements," *AIAA J.*, 47(8):1952–1964.
7. Arone, M., D. Cerniglia, and V. Nigrelli. 2006. "Defect characterization in Al welded joints by non-contact Lamb wave technique," *J. Mater. Process. Tech.*, 176(1):95–101.
8. Qiang, W. and Y. Shenfang. 2009. "Baseline-free imaging method based on new PZT sensor arrangements," *Journal of Intelligent Material Systems and Structures*, 20(14):1663–1673.
9. Sohn, H., H. W. Park, K. H. Law, and C. R. Farrar. 2007. "Combination of a time reversal process and a consecutiv outlier analysis for baseline-free damage diagnosis," *J. Intel. Mat. Syst. Str.*, 18(4):335–346.
10. McMechan, G. A. and M. J. Yedlin. 1981. "Analysis of dispersive waves by wave field transformation," *Geophysics*, 46(6):869–874.
11. Jiang, X., J. Lin, F. Ye, and F. Zheng. 2015. "Separation of P–P and P–SV wavefields by high resolution parabolic Radon transform," *J. Appl. Geophys.*, 119:192–201.
12. Foster, D. J. and C. C. Mosher. 1992. "Suppression of multiple reflections using the Radon transform," *Geophysics*, 57(3):386–395.
13. Ambrozinski, L., B. Piwakowski, T. Stepinski, and T. Uhl. 2014. "Evaluation of dispersion characteristics of multimodal guided waves using slant stack transform," *NDT & E. Int.*, 68:88–97.
14. Tran, T. N., K.-C. T. Nguyen, M. D. Sacchi, and L. H. Le. 2014. "Imaging ultrasonic dispersive guided wave energy in long bones using linear Radon transform," *Ultrasound Med. Biol.*, 40(11):2715–2727.
15. Yu, L. and V. Giurgiutiu. 2007. "In-situ optimized PWAS phased arrays for Lamb wave structural health monitoring," *J. Mech. Mater. Struct.*, 2(3):459–487.
16. He, J. and F.-G. Yuan. 2015. "Damage identification for composite structures using a cross-correlation reverse-time migration technique," *Struct. Health. Monit.*:1475921715602546.
17. He, J. and F.-G. Yuan. 2016. "A quantitative damage imaging technique based on enhanced CCRTM for composite plates using 2D scan," *Smart. Mater. Struct.*, 25(10):105022.
18. Lines, L. and S. Treitel. 1984. "Tutorial: A review of least-squares inversion and its application to geophysical problems," *Geophys. Prospect.*, 32(2):159–186.
19. Kabir, M. N. and K. J. Marfurt. 1999. "Toward true amplitude multiple removal," *The Leading Edge*, 18(1):66–73.